Long-range persistence of temperature records induced by long-term climatic phenomena

V. Capparelli,[1] A. Vecchio,[1] and V. Carbone[1,2]
[1]*Dipartimento di Fisica, Università della Calabria, Ponte P. Bucci Cubo 31 C, 87036 Rende (CS), Italy*
[2]*Liquid Crystal Laboratory, IPCF/CNR, Ponte P. Bucci Cubo 31C, 87036 Rende (CS), Italy*
(Received 21 April 2011; revised manuscript received 1 August 2011; published 7 October 2011)

The occurrence of persistence in climatic systems has been investigated by analyzing 1167 surface temperature records, covering 110 years, in the whole United States. Due to the nonlinear and nonstationary character of temperature time series, the seasonal cycle suffers from both phase and amplitude modulations, which are not properly removed by the classical definition of the temperature anomaly. In order to properly filter out the seasonal component and the monotonic trends, we define the temperature anomaly in a different way by using the empirical mode decomposition (EMD). The essence of this method is to empirically identify the intrinsic oscillatory modes from the temperature records according to their characteristic time scale. The original signal is thus decomposed into a collection of a finite small number of intrinsic mode functions (IMFs), having its own time scale and representing oscillations experiencing amplitude and phase modulations, and a residue, describing the mean trend. The sum of all the IMF components as well as the residue reconstructs the original signal. Partial reconstruction can be achieved by selectively choosing IMFs in order to remove trivial trends and noise. The EMD description in terms of time-dependent amplitude and phase functions overcomes one of the major limitation of the Fourier analysis, namely, a correct description of nonlinearities and nonstationarities. By using the EMD definition of temperature anomalies we found persistence of fluctuations with a different degree according to the geographical location, on time scales in the range 3–15 years. The spatial distribution of the detrended fluctuation analysis exponent, used to quantify the degree of memory, indicates that the long-term persistence could be related to to the presence of climatic regions, which are more sensitive to climatic phenomena such as the El Niño southern oscillation.

DOI: 10.1103/PhysRevE.84.046103 PACS number(s): 89.90.+n, 92.70.Gt, 05.40.−a, 92.70.Kb

I. INTRODUCTION

The short-term memory of many atmospheric parameters due to the stochastic dynamics of atmosphere is a well-known phenomenon. This allows the predictability of the meteorological parameters over weekly time scales. The variability at low time scales has been traditionally described by low-order autoregressive processes whose paradigm is the first-order autoregressive process

$$x_i = a x_{i-1} + \epsilon_i, \tag{1}$$

where x_i is the meteorological variable at time t_i, a is the first-order autocorrelation coefficient, and ϵ_i represents a Gaussian white noise. In particular, the parameter a introduces a rapid correlation decay so that the asymptotic behavior $x_i \sim \epsilon_i$ becomes uncorrelated and unpredictable starting from weekly scales. However, persistence has been found also at larger scales, related to the occurrence of "red" noise in the power spectra of long-time meteorological records [1–8]. At these scales the presence of memory could be related to the slow response of, e.g., oceans and ice cover or to climatic phenomena. For example, the weather is persistent when a very stable high-pressure system is established over a particular region remaining in place for several weeks, the so called "blocking" [9]. Persistence on monthly time scales has been related to slowly varying external forcing such as the sea surface temperature or intermittent phenomena in the solar-terrestrial system [5,10]. The presence of memory in the system has been inferred by using the usual detrended fluctuation analysis (DFA), obtained by investigating the scaling laws of fluctuations of detrended temperature anomalies, and in particular through a scaling exponent which indicates departures from a simple uncorrelated stochastic Brownian process [11].

The Earth surface temperature represents one of the most analyzed variables used to investigate the climatic system. Regarding the discussion of long-range correlation in temperature time series some aspects still remain open. First, Koscielny-Bunde *et al.* [2] proposed that the correlations should be universal, namely, not dependent on the geographic location of the analyzed station. The coupling of atmospheric and oceanic processes could be involved in setting the same exponent for long-range persistence for weather stations in different climatic zones and time regimes (from weeks to decades) [2]. The effects of this coupling, in the context of interdecadal and century-scale climate oscillations [12], is one of the core interests in climatology. More recently, the universality has been questioned since a wide range of exponent values seems to be present over continental lands [5,6,13] and marked differences seem to exist between land and sea surface temperatures [6,14,15]. The latter has been attributed to slowly varying external forcing such as the presence of oceans or even big reservoirs of water [6]. On the basis of some detailed data analysis, it has been emphasized that the value of the asymptotic power-law correlation exponent, obtained from the usual data sets, is not constant but instead depends on the scale [16]. This apparent scale invariance has been described through a simple bivariate Markov model accounting for the fractal behavior of the exponent [16]. Because of these discordant evaluations, the claimed universality of persistence still represents a matter of scientific debate [17,18].

Another aspect of whether or not the universality is valid concerns the geographic distribution of the correlation. In this

regard, the analysis of Australian temperatures indicates that the intensity of the asymptotic correlation seems to decrease with the distance from the equator [19]. Analysis of a more extended data set, acquired over the whole Earth, showed that correlations are grouped in large geographic areas which cannot be explained though a simple parametric dependence. In particular, the search for systematic dependence on the distance from the oceans gave negative results [5,7,19], while controversial results have been obtained for a dependence on elevation, for which increase [20], decrease [21], and absence [19] of correlation with the height have been found. Also, comparisons with global climate models lead to contrasting results. Seven state-of-the-art global models failed to reproduce the scaling behavior of long temperature records by underestimating the long-range correlation [3,4]. A better model performance regarding the possibility of reproduction of long-range correlations can be obtained by properly taking into account the atmosphere-ocean coupling [6] or by including volcanic forcing [22].

We remark that the presence or absence of persistence represents a very useful test for competing global climate models and to verify the basic assumptions underlying them [2], given that their reproductive power is important for interpretation of climate change predictions. Moreover investigation of the presence of memory in temperature records can contribute to the current debate over global warming and help to distinguish the anthropogenic signal from the fluctuations due to the natural variability of the geophysical system [23].

A key point in the calculation of the persistence concerns the presence of trends or trivial correlations in the raw temperature signal. In fact, trivial correlations are introduced by the annual seasonal cycle, while long-term correlations can be masked by trends that can be generated by anthropic processes, e.g., the well-known urban warming, the increase of concentration of gases in the atmosphere, etc. For these effect even uncorrelated data in the presence of long-term trends may appear correlated, and, on the other hand, long-term correlated data may look like uncorrelated data influenced by a trend. Usually, to remove trends and seasonal cycles the temperature anomalies are calculated. These are defined with respect to the seasonally varying mean value. That is, given a sequence of daily temperatures T_i, the anomalies ΔT_i are defined as the differences

$$\Delta T_i = T_i - \langle T_i \rangle, \tag{2}$$

where $\langle T_i \rangle$ represents the temperature mean value for the ith calendar day, averaged over a significantly large sample of data. Finally, ΔT_i should account for the effect of long-term climate change that should also be included in the definition of the anomaly. The implicit assumption that the seasonal annual cycle is constant and is generated by a set of stationary processes underlies the definition (2). The validity of that assumption is often questionable due to the nonlinear response of the climate system to external forcing. Both trends and irregularities in the seasonal cycle have been observed as changes of both amplitude [24] and phase [25–27] in the annual cycle of surface temperature. These effects are related to the complex nonlinear response of the atmosphere, land, and oceans to the periodic forcing provided by the annual motion of the Earth around the Sun [25,27] or to changes in albedo, soil moisture, and short-wave forcing [26]. The presence of irregularities of the seasonal cycle, if not suitably filtered, can introduce a fictitious statistical randomization, thus causing an artificial decrease of the persistence degree. Hence, because of the complex physics of the climatic system, the classical definition (2), based on the average, of temperature anomaly cannot be adequate and, as claimed by Thomson [25], "Anomaly series used in climate research that have been deseasonalized by subtracting monthly averages need to be recomputed. The best method for doing this is not obvious." As a consequence, the persistence estimation calculated starting from the definition (2) might be misleading and might lead to erroneous conclusions.

A different definition of temperature anomaly, based on the empirical mode decomposition (EMD), should be more suitable to take into account the nonstationarities related to changes of amplitude and phase of the seasonal cycle [8,28]. In particular, when the DFA was applied to very long European temperature records from Prague and Milan, a very similar degree of persistence was found, over a reduced range of scales (3–10 yr), by using the different definition of anomaly [8].

In the present paper we investigate the spatial distribution of the persistence degree of surface temperature in the United States in order to discuss its claimed universality and for a better understanding of the physical processes responsible for long-term persistence in climate. In particular, we compare the DFA results for temperature anomalies defined in the classical way (2) and through the EMD. The plan of the paper is the following: The data used and a different definition of temperature anomalies through the EMD are developed in Sec. II and results are presented in Sec. III. Finally some discussion and perspectives are given in Sec. IV.

II. DATA AND METHODS

We analyze the temperature records $T(t)$ from the United States Historical Climatology Network (HCN) [29]. The data set covers 110 years from 1898 up to 2008 and is recorded by $N = 1167$ different stations distributed on the whole United States. The N stations were selected in order to have homogeneous records characterized by the same duration and without gaps. The spatial distribution of the N station over the United States is reported in Fig. 1.

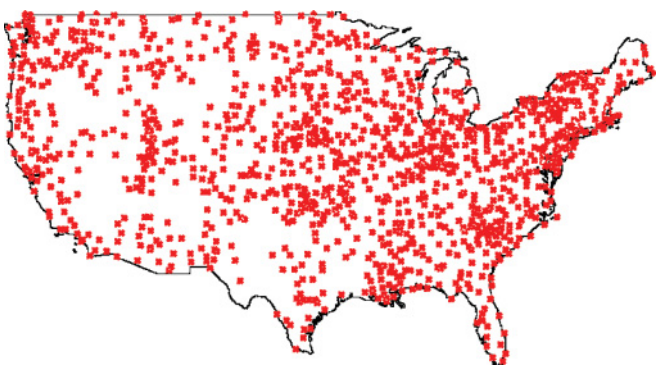

FIG. 1. (Color online) Spatial distribution of the stations.

A. Definition of temperature anomalies

The EMD has been developed to process nonstationary data [30] and successfully applied in many different contexts [31–34], including geophysical systems [28,35–37]. The EMD approach is more appropriate when dealing with nonstationary and nonlinear data like temperature records. In these cases the average operation, which critically depends on the chosen number of points, could cancel some of the relevant features in the original signal, thus reducing temporal resolution.

In the EMD framework a temperature record $T(t)$ is decomposed into a finite number n of intrinsic mode functions (IMFs) as

$$T(t) = \sum_{j=0}^{n-1} \theta_j(t) + r_n(t). \tag{3}$$

Each $\theta_j(t)$ has its own time scale and represents a zero-mean oscillation experiencing amplitude and frequency modulations, namely, it can be written as $\theta_j(t) = A_j(t)\cos\Phi_j(t)$, where $A_j(t)$ and $\Phi_j(t)$ represent respectively the amplitude and the phase of the jth EMD mode. This kind of decomposition is local, complete, and in fact orthogonal [30,38]. The residue $r_n(t)$ in (3) describes the mean trend. The statistical significance of information content for each IMF, with respect to a white noise, can be checked by applying a specific test based on the following argument [39]. When EMD is applied to a white noise series, the constancy of the product between the energy density of each IMF and its corresponding averaged period can be deduced. This relation can be used to derive the analytical energy density spread function of each IMF as a function of different confidence levels. Thus, by comparing the energy density of the IMFs extracted from the actual data with the theoretical spread function, one can distinguish IMFs containing information at the selected confidence level from purely noisy modes. The temperature record filtered for trends and for the seasonal cycle can be obtained by exploiting the orthogonality of EMD modes and reconstructing the signal through the partial sums in (3) [28,30,40]. The orthogonality of IMFs guarantees that each j mode captures a single aspect of the complex dynamics of the system. Thus it is meaningful to split the temperature signal into three parts, namely, a seasonal contribution $S(t)$, the anomaly $\Delta T(t)$, and the residue $r_n(t)$,

$$T(t) = S(t) + \Delta T(t) + r_n(t). \tag{4}$$

For the analyzed data set the residue $r_n(t)$ represents the monotonically increasing local trend of temperature, commonly attributed to large-scale warming since the urbanization contribution is smaller [41].

By looking at the IMFs, identified by the index $j = 0,1,\ldots,n-1$, we can define two mutually orthogonal sets of indices s and r, such that each $j \in s \oplus r$. Then, by partial sums, we can reconstruct the seasonal contribution by using only the subset s, that is,

$$S(t) = \sum_{j\in s} \theta_j(t), \tag{5}$$

while the remaining IMFs, belonging to the set r, are used to define temperature anomalies [8]

$$\Delta T(t) = \sum_{j\in r} \theta_j(t). \tag{6}$$

Due to the complexity of the system, the sets r and s cannot be defined *a priori*; rather, they are suitably chosen by looking at the time behavior of the various IMFs.

The EMD analysis of the monthly historical Prague and Milan temperature records [8,27] indicates that the the first IMF, $\theta_0(t)$, is associated with the weather vagaries at monthly scales, and the seasonal cycle for the Milan data set is captured by the mode $\theta_1(t)$, characterized by a typical time scale of $\Delta\tau_1 \simeq 1$ yr. On the other hand, the seasonal cycle of the Prague data set presents an irregular behavior. In fact, $\theta_1(t)$ shows a regular seasonal oscillation interrupted by a few intermittent local decreases of the amplitude, and the full seasonal cycle is obtained when $\theta_1(t)$ and $\theta_2(t)$ are summed up. The same features are observed in the US HCN data set analyzed in this paper. Almost 66% of the stations present an irregular seasonal cycle, while the remaining 34% of the stations show a regular seasonal oscillation whose contribution is isolated in $\theta_1(t)$. As an example we report in Fig. 2 the time behavior of the mode $\theta_1(t)$ from both the Holly, CO and Covington, LA stations, which are characterized by regular and anomalous seasonal oscillations, respectively. In Fig. 3 the time evolutions of $\theta_1(t)$ and $\theta_2(t)$ [Figs. 3(a) and 3(b)] and their sum [Fig. 3(c)], for the Covington, LA temperature record, are shown over a restricted time interval of about 25 yr. As discussed in Ref. [27] the seasonal irregularities found in temperature records do not occur randomly in time; their occurrence regularly oscillates with a period of 18.6 yr. Moreover, a strong phase coherence between the irregularity occurrence and the inclination of the Moon's orbit with respect to the equatorial plane, due to nutation, has been reported [27]. These observations indicate a possible connection between the Earth's nutation and the occurrence of irregularities by means of modulation in the insolation and/or tidal effects. We verified that the seasonal irregularities cannot be fully eliminated and

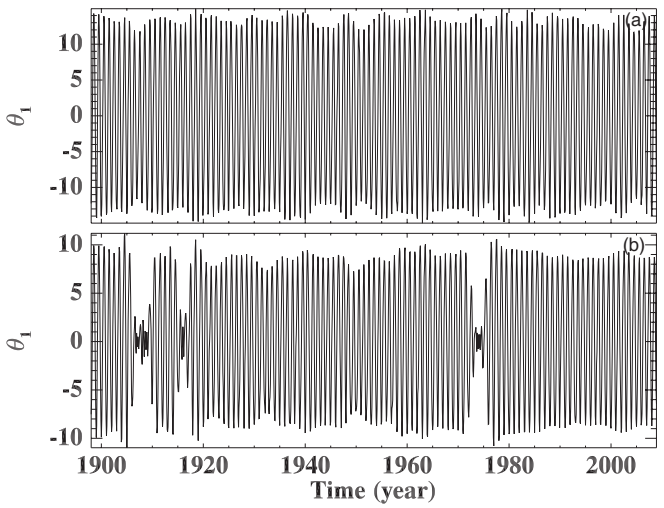

FIG. 2. Time evolution of the EMD modes $j = 1$ for the temperature records of Holly, CO (a) and Covington, LA (b).

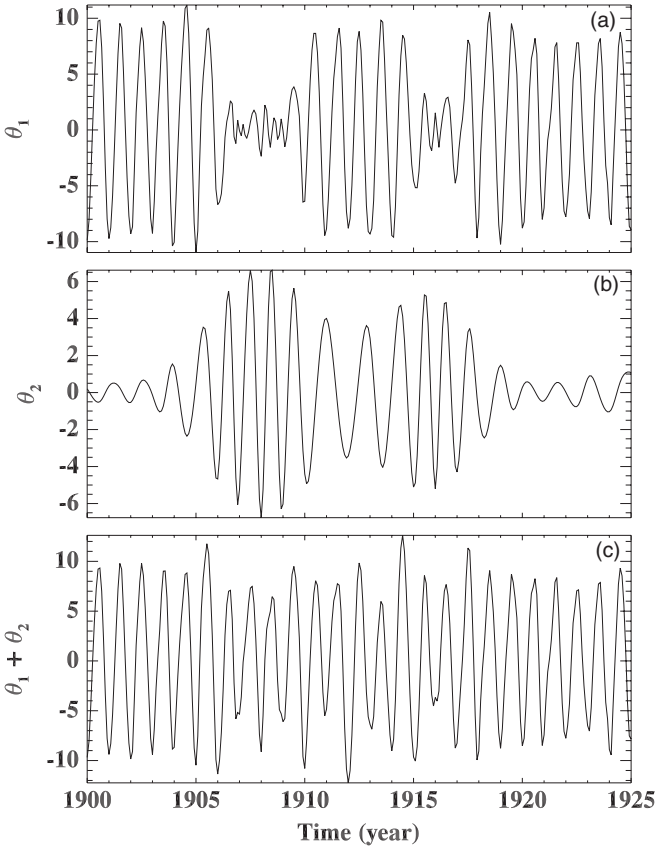

FIG. 3. Time evolution of the EMD modes $j = 1$ and $j = 2$ (a), (b) and their sum (c) for the temperature record of Covington, LA.

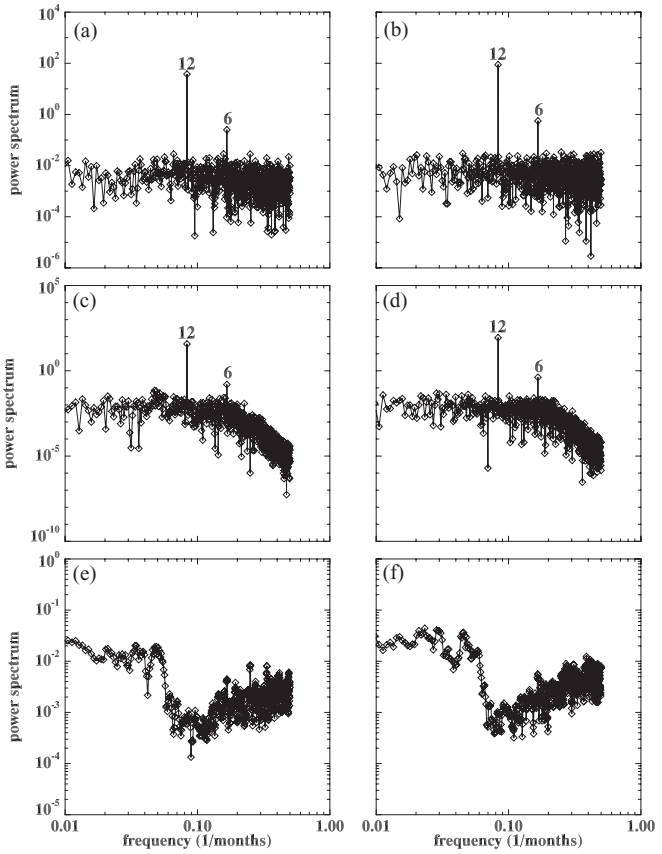

FIG. 4. Top panels: Fourier power spectra of (a) Holly, CO and (b) Covington, LA temperature records. Middle panels: Fourier spectra of seasonal oscillation given by (c) the EMD mode $j = 1$ for Holly, CO and (d) the sum of modes $j = 1$ and $j = 2$ for Covington, LA. Bottom panels: Fourier spectra of the temperature anomalies for (e) Holly, CO and (f) Covington, LA. The numbers over the peaks indicate the corresponding periodicity in months.

the main results of this paper remain unchanged when the noise-assisted method named ensemble EMD (EEMD) [33] is used. The latter has been developed, in signal processing, to achieve signal cleanliness by removing irregularities, thus obtaining regular modes. We remark that, in the case discussed in this paper, the EEMD approach does not seem suitable since the cancellation of the irregularities from IMFs could mask important physical aspects of the phenomenon at hand.

As far as the definition of temperature anomaly is concerned, the presence of irregularities in the seasonal cycle enforces the need for a different definition of anomaly. In fact nonstationary periods, present in the temperature records, could affect the regular seasonal oscillation. Taking care of the above considerations, the most natural way to define temperature anomalies is to consider the contribution of all EMD modes except for the properly defined seasonal oscillation. The latter contribution, as we said before, can be different according to the record analyzed. Thus the set r in (6) represents the collection of EMD modes such that $r = \{j | \, 0 \leqslant j \leqslant n-1\} \ominus \{j = 1\}$ in the case of a regular seasonal cycle (as for example in Holly, CO), and $r = \{j | \, 0 \leqslant j \leqslant n-1\} \ominus \{j = 1,2\}$ in the case of an irregular seasonal cycle (as for example in Covington, LA). With this choice, the seasonal cycle, which could present amplitude and phase variations, is more properly excluded by the definition of temperature anomalies.

Fourier power spectra of $S(t)$ from Holly, CO [Fig. 4(c)] and Covington, LA [Fig. 4(d)] show the seasonal cycle isolated by the EMD. The Fourier spectra of $\Delta T(t)$ for both Holly, CO and Covington, LA records are reported in Figs. 4(e) and 4(f). Note that temperature anomalies defined through the EMD can be considered as deseasonalized at a very good approximation.

B. Analysis of persistence

To investigate the persistence in the analyzed records, we used the detrended fluctuation analysis which consists of some standard steps. First of all from a sequence of anomalies of length N we extract y_k defined as

$$y_k = \sum_{i=1}^{k} \Delta T_i. \tag{7}$$

y_k is then divided into boxes of equal time length t_n and in each box a polynomial curve of order p is fitted, thus obtaining the local trend $y_k^p(t_n)$. The detrended signal $s_k^{(p)}(t_n) = y_k - y_k^p(t_n)$ is calculated for each box, and the usual measure of fluctuation

is given by the standard deviation of the detrended segment averaged over all the boxes:

$$F_p(t_n) = \sqrt{\frac{1}{N}\sum_{k=1}^{N}\left[s_k^{(p)}(t_n)\right]^2}. \quad (8)$$

A scaling exponent δ_p is then defined through the power-law relationship $F_p(t_n) \sim t_n^{\delta_p}$. It can be shown that a process for which the power-law relationship exists has also a power-law autocorrelation function $C(\tau) = \langle \Delta T_i \Delta T_{i+\tau} \rangle \sim \tau^{-\alpha}$ (where $0 < \alpha < 1$) and a frequency spectrum given by $S(f) \sim f^{-\beta}$ (where $0 < \beta < 1$). The scaling exponents are related to the DFA index through $\alpha = 2(1 - \delta_p)$ and $\beta = 2\delta_p - 1$ [2,42]. Thus, a scaling exponent $\delta_p = 1/2$ is associated with uncorrelated Brownian-like stochastic processes and separates a persistent process where $\delta_p > 1/2$ from an antipersistent process where $\delta_p < 1/2$. According to previous analysis [16–19] we use the DFA2, namely, $p = 2$ in (8). To reduce the noise level the standard "sliding window" technique, where local trend removal and variance computation were performed by choosing each possible starting values for a given box of length t_n, was applied [19].

III. RESULTS

Since the stations we investigate cover the whole United States in a rather uniform way, we will focus on the spatial properties of the persistence and discuss the differences obtained when the anomalies are defined in the classical way or through the EMD. The asymptotic DFA2 exponent can be used as a proxy for the presence of long-range effects not attributable to the intrinsic atmospheric fluctuations. In particular, we fitted the scaling relation $F_2(t_n) \sim t_n^{\delta_2}$ in the range of scales $3 \leqslant t_n \leqslant 15$ yr. This range was chosen in order to directly compare our results with the cases studied in previous papers [8,18,19]. The uncertainties $\delta F_p(t_n)$ can be estimated from the uncertainties on $\delta s_k^{(p)}$, using definition (8), as

$$\delta F_p(t_n) = \frac{\delta s_k^{(p)}}{2\sqrt{F_p(t_n)}}, \quad (9)$$

where $\delta s_k^{(p)}$ has been evaluated as the standard deviation of $[s_k^{(p)}(t_n)]^2$ over the boxes. When the anomalies are defined in the standard way (2), the χ^2 probability of the fit is below 0.6 for about 16% of stations, while this number increases to 37% when anomalies are calculated according to our definition through EMD. This means that, for some records, the accuracy of the fit is insufficient in the chosen range of scales, that is, the persistence does not extend to longer periods. For these stations the accuracy level of the fit was increased by reducing the upper value of t_n up to 7 yr in order to reach an acceptably high accuracy (χ^2 probability $\geqslant 0.6$) for all records. An example of the DFA2 curves for both Holly, CO and Covington, LA stations is shown in Fig. 5 where black and red lines refer to EMD and the classically defined temperature anomaly, respectively.

The statistics of the DFA2 exponent is shown in Fig. 6, where the histograms of δ_2 [Fig. 6(a)] and its uncertainty $\Delta\delta_2$ [Fig. 6(b)] are reported for both definitions of the

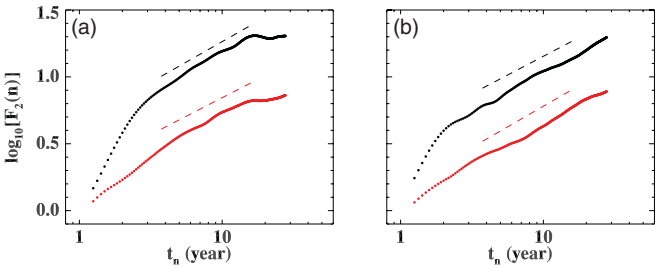

FIG. 5. (Color online) The scaling function $F_2(n)$ as a function of the temporal scale n for Holly, CO (a) and Covington, LA (b) stations. Black (upper) and red (lower) lines refer to EMD and classically defined temperature anomaly, respectively. Straight lines correspond to linear fits.

anomalies. The values of δ_2, for classical anomalies, are shifted toward lower values with respect to the persistence obtained when anomalies are defined through EMD. In particular, δ_2 values lower than 0.6 were detected for 40% of stations when anomalies are defined according to (2), while these values are detected in 16% of stations when EMD is used. This result indicates that the EMD reveals a long-range positive correlation in the majority of the United States. This means that the classical definition of the temperature anomaly underestimates the degree of persistence, due to the randomization caused by stochastic fluctuations in the seasonal cycle, which are not suitably filtered by the assumed constant seasonality in the classical definition. Both distributions of the uncertainties are sharply peaked around $\Delta\delta_2 \simeq 0.01$. We remark that this value is slightly lower than the error estimates performed by in the past [6,19] by using different approaches in the uncertainty evaluation.

A comparison between the geographic distribution of the DFA2 exponents is shown in Fig. 7 where the δ_2 maps are reported for both the anomalies defined in the classical way [Fig. 7(a)] and through the EMD [Fig. 7(b)]. The maps have been built by computing the Voronoi polygon of each station, namely, the polygon containing the region closer to that point than to any other point. Figure 7 clearly indicates that the correlation exponent is far from being universal in continental locations. For both maps the strength of the long-range correlation is distributed in large geographic patches, with substantial differences. In particular, Fig. 7(a) shows two opposite patches of high and low degrees of persistence. The second one is concentrated in the Rocky Mountains area where

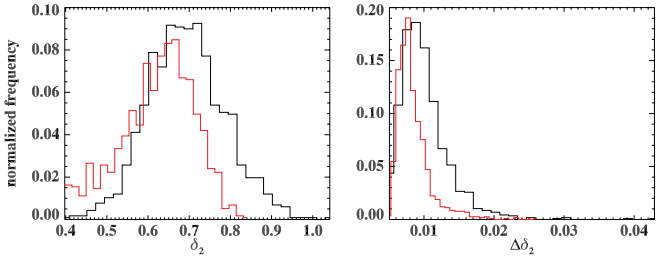

FIG. 6. (Color online) Normalized histogram of (a) DFA2 exponents and (b) their uncertainty calculated through the classical (thin red line) and EMD (thick black line) definition of the temperature anomaly.

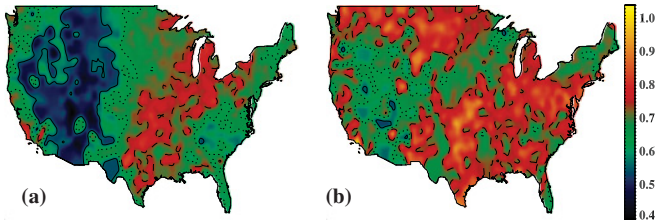

FIG. 7. (Color online) Geographic distribution of the DFA2 exponent δ_2 of (a) classical and (b) EMD definition of the temperature anomaly. Solid, dotted, and dashed lines refer to levels 0.5, 0.6, and 0.7, respectively.

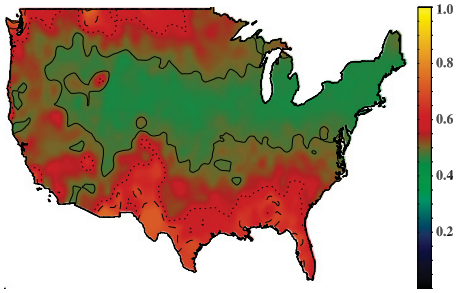

FIG. 8. (Color online) Normalized amplitude of the 24-month harmonic fit to the ENSO temperature composites (see the text for details). Solid, dotted, and dashed lines refer to levels 0.5, 0.7, and 0.9, respectively.

the height of the stations exceeds 1200 m. This result, however, is inconsistent with a linear dependence on the elevation since the correlation drops at the sea level while its maximum is located in a region where the average height of the stations is about 240 m [19]. The map reported in Fig. 7(b) shows a more uniform distribution of the persistence index with higher values in two large areas, the first enclosed by the Atlantic Ocean and the Gulf of Mexico, namely, the southeastern United States, and the second in the northwest part of the United States. We remark that the EMD identifies large values of persistence in the coastal areas, an expected result given the ocean's inertia. As in the map of Fig. 7(a), lower values of δ_2 are concentrated in the region of the Rocky Mountains. The latter result is in agreement with the findings of Ref. [43] which show that the decorrelation of climate records is much stronger for the mountain stations. This effect could be due to the influence of free atmospheric dynamics such as low-lying clouds and/or latent heat exchange of the surface [43].

The pattern of persistence obtained from the classical anomaly is quite complex; it does not allow any simple correlation with long-term climatic phenomena and does not show a parameter dependence (e.g., distance from oceans and/or elevation). On the other hand, the map obtained from the EMD anomaly allows an easier interpretation. In fact, we can recognize climatic regions through iso-δ_2 surfaces. In particular, the spatial pattern suggests that the observed correlations in the temperatures could be induced by climatic phenomena. For example, it is well known that the El Niño southern oscillation (ENSO) influences surface temperature at regional scales [44,45]. The areas of high persistence values in Fig. 7(b) roughly correspond to the Unites States regions showing a clearly defined (at the 99% significance level) ENSO-temperature relationship (see Fig. 8 from [44], Fig. 6 from [45], and the figure [46]). The latter regions can be identified by using the method designed by the authors of Refs. [44,45]. In detail, the montly temperature data for each station were ranked and the ENSO composite ranks were formed for the two-year interval including an ENSO episode. For each temperature record 27 ENSO events, as identified from Refs. [47,48], have been considered. The first harmonic was extracted from the 2 yr ENSO composite series and its amplitude and phase were calculated. Both these quantities, when plotted on the United States map, indicate the magnitude and the phase of the response to the ENSO episode. A coherence map can also be built in order to underline the areas having a coherent response to the ENSO events. Figure 8 represents the normalized amplitude of the 24-month harmonic fit to the ENSO temperature composites. We remark that in the areas of high amplitude the coherence is greater than 0.9. Roughly speaking, Fig. 8 indicates the geographic areas in which the temperature records have a stronger and coherent ENSO response [44,45]. A comparison between Figs. 7(b) and 8 indicates that the areas of higher persistence values and higher temperature-ENSO response are similarly distributed in the southeastern and, mainly, in the northwestern United States. The temperature response to the ENSO in North America can be related to the presence of tropical forcing of the circulation pattern, in particular to the Pacific-North American circulation pattern (PNA), induced by the forcing of the mid-latitude circulation [44]. Our results indicate that long-term persistence could be induced by the ENSO on the surface temperatures, similarly to the relation between the ENSO and sea surface temperature [15]. We note the presence of a persistence patch on the east side in a narrow area enclosed between the Atlantic Ocean and the Great Lakes region not observed in the ENSO-temperature response map (Fig. 8). It could be related to the North Atlantic oscillation (NAO), which represents one of the most prominent and recurrent patterns of atmospheric circulation variability, driving decadal climate variability and trends from the eastern seaboard of the United States to the whole of Europe [49], and/or to the simultaneous nearness of the water reservoirs of the Great Lakes and Atlantic Ocean. The possibility of highlighting a meaningful persistence pattern, possibly related to long-term climatic phenomena which induce correlations in the system, seems to be a prerogative of the EMD-defined temperature anomaly. This could depend on the inadequacy of the classical definition of the temperature anomaly in the presence of quasiperiodic climate patterns, like the ENSO, whose signal could be aliased by averages over the calendar day [45].

Other information is provided by the map in Fig. 9 showing the spatial distribution of the upper value of t_n chosen for the DFA fit so that the χ^2 probability exceeds 0.6, in the case of the temperature anomaly defined through the EMD. Lower values are concentrated in a large area in the northwest and in smaller patches distributed in the southeast United States. The high values of persistence in the northwest are found in a narrow range of scales, namely, $3 \leqslant t_n \leqslant 7$ yr, which also corresponds to the typical periods of the ENSO phenomenon. This represents a further indication that in this

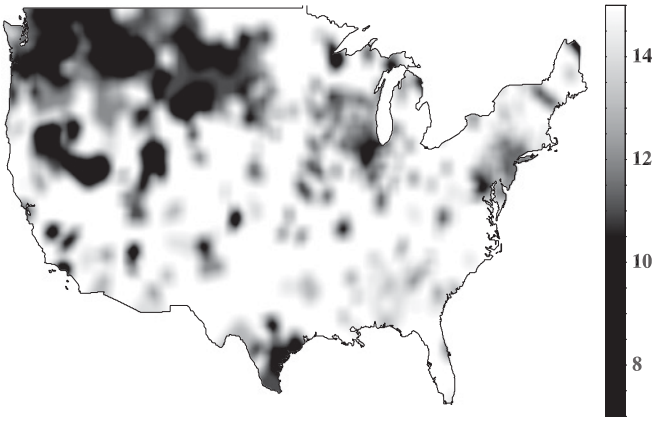

FIG. 9. Geographic distribution of the upper t_n value, in years, used for the DFA fit, for temperature anomalies defined through the EMD.

area the persistence could be related to the correlations induced by the ENSO. The southeast region, also characterized by a high temperature-ENSO response, shows high persistence in a slightly larger range of time scales, namely, $3 \leqslant t_n \leqslant 15$ yr. This could indicate that the correlations found are also related to other effects, such as the NAO or the water reservoir due to the lakes and ocean, acting with the ENSO in this area.

IV. CONCLUSIONS

In the present paper we investigated the persistence of surface temperature anomalies within the United States. We introduced a different definition of temperature anomaly, based on the EMD expansion of temperature records in empirical IMFs.

In fact, due to the presence of trends in the temperature records and phase-amplitude fluctuations in the seasonal component, the latter is badly filtered out when using the usual definition (2) of temperature anomalies [8,27,28]. On the other hand, the introduced temperature anomalies properly filter out a seasonal component which varies in both amplitude and phase. Spurious stochasticity introduced in the system by this effect is filtered out from the temperature anomalies so that the persistence can be properly calculated. The latter has been estimated through the DFA2 scaling exponent δ_2 which indicates departure from a Brownian memoryless stochastic process.

Temperature anomalies defined through the EMD show higher values with respect to δ_2 calculated through the classical definition of anomaly. We found that long-term persistence clearly exists at time scales in the range $3 \leqslant t_n \leqslant 15$ yr with a different degree of persistence according to the geographical location. The uncertainty associated with the scaling exponents δ_2, calculated in a statistical way during the DFA computation, is lower than the error estimates discussed in the literature [6,19].

Our analysis indicates that the long-term persistence can be related to the regional effect of climatic phenomena. In fact, the spatial pattern of the scaling exponents, obtained by using the EMD definition of temperature anomalies, reflects areas showing a stronger ENSO-temperature relationship. By reversing the point of view, we can say that the spatial distribution of the persistence degree provides a quantitative way to discriminate among the different climatic regions. To this purpose we note that, as suggested by an anonymous referee, the areas of higher persistence in Fig. 7(b) appear similar to the climate zones of the United States (lower map in Ref. [50]). It is well known that decadal climatic phenomena, like the ENSO, influence surface temperatures in the southeast and northwest parts [44–46] of the United States. We found that the northwest region manifests a strong persistence in the range of scales $3 \leqslant t_n \leqslant 7$ yr, namely, the typical time scales of the ENSO. The southeast regions manifest persistence over a slightly greater range of scales, namely, at $3 \leqslant t_n \leqslant 15$ yr. This indicates that in the latter regions other effects, such as the NAO or the water reservoir, could operate with the ENSO in inducing correlations. The results obtained when EMD-defined temperature anomalies are used, e.g., the presence of a meaningful persistence spatial pattern, depend on an estimate of the temperature anomalies where the amplitude- and phase-modulated seasonal component and the local trends can be suitably removed and thus do not mask the presence of long-term climatic phenomena which induce persistence.

ACKNOWLEDGMENTS

We acknowledge two anonymous referees for useful comments.

[1] P. D. Ditlevsen, H. Svensmark, and S. Johnsen, Nature (London) **379**, 810 (1996).
[2] E. Koscielny-Bunde, A. Bunde, S. Havlin, H. E. Roman, Y. Goldreich, and H.-J. Schellnhuber, Phys. Rev. Lett. **81**, 729 (1998).
[3] J. Syroka and R. Toumi, Geophys. Res. Lett. **28**, 3255 (2001).
[4] R. B. Govindan, D. Vyushin, A. Bunde, S. Brenner, S. Havlin, and H.-J. Schellnhuber, Phys. Rev. Lett. **89**, 028501 (2002).
[5] J. F. Eichner, E. Koscielny-Bunde, A. Bunde, S. Havlin, and H.-J. Schellnhuber, Phys. Rev. E **68**, 046133 (2003).
[6] K. Fraedrich and R. Blender, Phys. Rev. Lett. **90**, 108501 (2003).
[7] A. Király, I. Bartos, and I. M. Jánosi, Tellus A **58**, 593 (2006).
[8] A. Vecchio and V. Carbone, Phys. Rev. E **82**, 066101 (2010).
[9] J. G. Charney and J. Devore, J. Atmos. Sci. **36**, 1205 (1979).
[10] N. Scafetta and B. J. West, Phys. Rev. Lett. **90**, 248701 (2003).
[11] C.-K. Peng, S. V. Buldyrev, S. Havlin, M. Simons, H. E. Stanley, and A. L. Goldberger, Phys. Rev. E **49**, 1685 (1994).
[12] M. E. Mann, J. Park, and R. S. Bradley, Nature (London) **378**, 266 (1995); P. Chang, L. Ji, and H. Li, *ibid.* **385**, 516 (1997); R. T. Sutton and M. R. Allen, *ibid.* **388**, 563 (1997).
[13] M. L. Kurnaz, J. Stat. Mech. (**2004**) P07009.

[14] K. Fraedrich, U. Luksch, and R. Blender, Phys. Rev. E **70**, 037301 (2004).
[15] R. A. Monetti, S. Havlin, and A. Bunde, Physica A **320**, 581 (2003).
[16] M. Lanfredi, T. Simoniello, V. Cuomo, and M. Macchiato, Atmos. Chem. Phys. **9**, 4537 (2009).
[17] A. Bunde, J. F. Eichner, S. Havlin, E. Koscielny-Bunde, H.-J. Schellnhuber, and D. Vyushin, Phys. Rev. Lett. **92**, 039801 (2004).
[18] K. Fraedrich and R. Blender, Phys. Rev. Lett. **92**, 039802 (2004).
[19] A. Kiràly and I. M. Jánosi, Meteorol. Atmos. Phys. **88**, 119 (2005).
[20] M. N. Efstathiou and C. A. Varotsos, Int. J. Remote Sensing **31**, 343 (2010).
[21] Y. Liu and R. Avissar, J. Clim. **12**, 2154 (1999).
[22] D. Vyushin, I. Zhidkov, S. Havlin, A. Bunde, and S. Brenner, Geophys. Res. Lett. **31**, L10206 (2004).
[23] *Climate Change 1995: The Science of Climate Change*, edited by J. T. Houghton *et al*. (Cambridge University Press, Cambridge, England, 1996).
[24] C. Wallace and T. Osborn, Clim. Res. **22**, 1 (2002).
[25] D. J. Thomson, Science **268**, 59 (1995).
[26] A. R. Stine, P. Huybers, and I. Y. Fung, Nature (London) **457**, 435 (2009).
[27] A. Vecchio, V. Capparelli, and V. Carbone, Atmos. Chem. Phys. **10**, 9657 (2010).
[28] Z. Wu, E. K. Schneider, B. P. Kirtman, E. S. Sarachik, N. E. Huang, and C. J. Tucker, Clim. Dyn. **31**, 823 (2008).
[29] The HCN data set is available at [http://cdiac.ornl.gov/epubs/ndp/ushcn/ushcn.html].
[30] N. E. Huang *et al*., Proc. R. Soc. London, Ser. A **454**, 903 (1998).
[31] J. Jamsek, A. Stefanovska, P. V. E. McClintock, and I. A. Khovanov, Phys. Rev. E **68**, 016201 (2003).
[32] A. Hutt, A. Daffertshofer, and U. Steinmetz, Phys. Rev. E **68**, 036219 (2003).
[33] Z. Wu and N. E. Huang, Adv. Adapt. Data Anal. **1**, 1 (2009).
[34] M. D. Alexandrov, A. Marshak, B. Cairns, A. A. Lacis, and B. E. Carlson, Geophys. Res. Lett. **31**, L04118 (2004).
[35] I. M. Jánosi and R. Müller, Phys. Rev. E **71**, 056126 (2005).
[36] J. I. Salisbury and M. Wimbush, Nonlin. Proc. Geophys. **9**, 341 (2002).
[37] L. Zhen–Shan and S. Xian, Meteorol. Atmos. Phys. **95**, 115 (2007).
[38] D. A. T. Cummings, R. A. Irizarry, N. E. Huang, T. P. Endy, A. Nisalak, K. Ungchusak, and D. S. Burke, Nature (London) **427**, 344 (2004).
[39] Z. Wu and N. E. Huang, Proc. R. Soc. London, Ser. A **460**, 1597 (2004).
[40] A. Vecchio, M. Laurenza, V. Carbone, and M. Storini, Astrophys. J. **709**, L1 (2010).
[41] T. C. Peterson, J. Clim. **16**, 2941 (2003); D. E. Parker, *ibid*. **19**, 2882 (2006); P. D. Jones, D. H. Lister, and Q. Li, J. Geophys. Res. Atmos. **113**, 16122 (2008).
[42] P. Talkner and R. O. Weber, Phys. Rev. E **62**, 150 (2000).
[43] R. O. Weber and P. Talkner, J. Geophys. Res. **106**, 20131 (2001).
[44] C. F. Ropelewski and M. S. Halpert, Mon. Wea. Rev. **114**, 2352 (1986).
[45] M. S. Halpert and C. F. Ropelewski, J. Clim. **5**, 577 (1992).
[46] NOAA National Climatic Data Center Paleoclimatology, [http://www.ncdc.noaa.gov/paleo/ctl/clisci10c.html], adapted from Fig. 6 of Ref. [45].
[47] E. M. Rasmusson and T. H. Carpenter, Mon. Weather Rev. **111**, 517 (1983).
[48] The data for the warm and cold ENSO episodes from 1951, collected by NOAA, are available at [http://www.cpc.ncep.noaa.gov/products/analysis_monitoring/ensostuff/ensoyears.shtml].
[49] J. W. Hurrell, Y. Kushnir, G. Ottersen, and M. Visbeck, Geophys. Monograph **134**, 1 (2003).
[50] US Energy Information Administation Climate Zones map, records 1978–2005 [http://www.eia.gov/consumption/residential/methodology/index.cfm].